\$ SUPER

Contents lists available at ScienceDirect

European Journal of Pharmaceutics and Biopharmaceutics

journal homepage: www.elsevier.com/locate/ejpb





Characterisation of skin penetration pathways using stimulated Raman scattering microscopy

Anukrati Goel^a, Ruth Pendlington^b, Stephen Glavin^b, Tao Chen^a, Natalie A. Belsey^{a,c,*}

- ^a School of Chemistry and Chemical Engineering, University of Surrey, Guildford GU2 7XH, UK
- ^b Unilever Safety & Environmental Assurance Centre, Colworth Science Park, Bedford MK44 1LQ. UK
- ^c Chemical & Biological Sciences Department, National Physical Laboratory, Hampton Road, Teddington TW11 OLW, UK

ARTICLE INFO

Keywords: Stimulated Raman scattering microscopy Topical drug delivery Cutaneous absorption Raman spectroscopy

ABSTRACT

Understanding the mechanisms governing the penetration of substances into the skin is crucial for the development of safe and effective topical drug delivery systems and skincare products. This study examined the partitioning of model permeants into human skin, by assessing six substances with diverse logP values. We employed stimulated Raman scattering (SRS) microscopy, an ambient, label-free optical imaging technique known for its ability to provide chemical distribution with subcellular resolution. Our investigation assessed partitioning into the two primary pathways through which substances traverse the skin: the intercellular lipid matrix and the intracellular route via corneocyte cells. We observed that the partitioning behaviour was strongly influenced by the lipophilicity of the molecule, with lipophilic compounds showing greater affinity for intercellular matrix with increased lipophilicity. Conversely, hydrophilic molecules demonstrated a preference for corneocyte cells, with their affinity increasing with increased hydrophilicity. The findings contribute to our understanding of the mechanisms underlying topical delivery and offer important implications and new methods beneficial for the development of safe and effective topical products. In addition, the methods presented could be valuable to reveal changes in drug partitioning or to assess targeting approaches in diseased skin models.

1. Introduction

Human skin serves as a versatile medium for delivering various compounds in dermatological, cosmetic, and pharmaceutical contexts, while simultaneously acting as a barrier to regulate the passage of substances into the skin. At the forefront of this barrier lies the stratum corneum (SC), the outermost layer of the skin, which serves as the principal interface between the body and the external environment [1]. SC is a complex tissue with tightly packed layers of keratin filled corneocyte cells embedded in intercellular lamellar lipids composed of ceramides, fatty acids, and cholesterol [2]. Given the heterogeneity of tissue, SC provides various penetration mechanisms which have been a subject of intense research, driven by the need to develop effective strategies for topical drug delivery and skincare formulations [3,4].

Traditional bulk methods for studying skin permeation, such as *invitro* permeation testing, or adhesive tape stripping, provide very limited mechanistic information. Spontaneous Raman spectroscopy is typically too time-consuming to generate images with sufficient spatial resolution [5,6] necessary to discern specific pathways within the skin, while

fluorescent microscopies are dependent on the use of fluorescent probes, which when conjugated, significantly perturb the uptake of small molecules [7]. However, the advent of advanced imaging techniques, notably stimulated Raman scattering (SRS) microscopy, has enabled the characterization of chemical distribution within the skin at a subcellular level [8,9]. Leveraging the vibrational properties of chemical bonds, SRS imaging offers rapid, label-free and non-invasive imaging capabilities for visualising the distribution of molecules within biological samples [10]. Additionally, the direct proportionality between SRS signal intensity and molecular concentration enables straightforward analysis, consolidating SRS microscopy as a robust and at least semi-quantitative method for chemical imaging. These unique features make SRS imaging particularly well-suited for studying skin permeation and unravelling the intricate mechanisms through which substances penetrate the skin barrier [11]. The excellent imaging ability of SRS in skin research was first demonstrated by Saar et al. in 2011 [12] where they observed the permeation of ketoprofen in murine skin through intercellular lipids of SC as well as through hair shafts. Another study by Wei et al. [13] visualized the permeation of antifungal drug terbinafine hydrochloride

E-mail address: n.belsey@surrey.ac.uk (N.A. Belsey).

^{*} Corresponding author.

in the skin of mouse ears through lipids, consistent with its lipophilic nature. In a complementary approach [14], Chen et al. explored permeation pathways in excised human skin using coherent anti-Stokes Raman scattering microscopy [15] combined with two-photon excited auto-fluorescence, offering additional insights into chemical distribution. Their observations revealed the preferential localization of hydrophobic jasmonic acid within lipid membranes, whereas hydrophilic glycerol appeared to be concentrated in both cell bodies and membranes, which was also validated by Saari et al. [16] in in-vivo human skin. Belsey et al. [17] tracked the visualization of ibuprofen in porcine skin using SRS, observing drug deposition as well as crystallization within the skin. Most recently Feizpour et al. [18] employed depth and time-resolved SRS imaging to investigate the permeation dynamics of an anti-inflammatory hydrophobic drug in mouse skin. Their study elucidated the drug's accumulation in lipid-rich regions, quantified through partition factor calculations, providing valuable quantitative insights into permeation mechanisms.

Despite these notable contributions, a knowledge gap remains regarding the permeation mechanisms of molecules spanning a wide range of physicochemical properties, in particular their hydrophobicity. Moreover, most studies have been conducted using animal skin models, which may not be representative of human skin physiology [19]. In this context, Choe et al.'s research [20] emphasized the importance of utilizing human skin for studying skin physiology and topical delivery, highlighting its higher barrier function compared to animal skin models.

To address these knowledge gaps, this study employed SRS to investigate chemical uptake into human skin across a range of molecules, featuring diverse partition coefficients (-0.92 to 7.71) and molecular weights (84.0 to 328.0). Specifically, six molecules namely deuterated palmitic acid (d-PA), terbinafine hydrochloride (TBF), 4-cyanophenol (4CP), deuterated fumaric acid (d-FA), caffeine (CAF) and

deuterated propylene glycol (d-PG) — were investigated following their topical application. The chemical structures, along with their respective logP and molecular weights, are depicted in Fig. 1.

The selection of these active compounds is motivated by their relevance to dermatological [21,22] or pharmaceutical [23,24] applications and their diverse logP values, ranging from highly hydrophobic (logP 7.71) to relatively hydrophilic (logP -0.92). Furthermore, these molecules possess unique spectral signatures that do not overlap with endogenous skin signals and therefore do not necessitate disentanglement from superimposed signals [25]. In pursuit of delineating mechanistic pathways of chemical penetration, the differential uptake in lipidrich and lipid-poor regions is compared to quantify partitioning across different routes. Such findings hold immense potential for advancements in the development of safe and effective topical formulations for pharmaceutical delivery and consumer health products.

2. Materials and methods

2.1. Preparation of formulations

4CP, d₈-PG, d₃₁-PA, TBF, CAF, d₂-FA were purchased from Sigma Aldrich, UK. A 70 mg/ml 4CP solution, 50 mg/ml TBF solution and 25 mg/ml d-FA solution were prepared in a vehicle of equi-volume propylene glycol (PG) (MP Biomedicals, UK) and ultrapure water. A 30 mg/ml caffeine solution was prepared in ultrapure water. A 38 mg/ml d-PA was prepared in a vehicle of 100 % PG while an equi-volume solution of d-PG and ultrapure water was prepared to analyse d-PG in skin. The prepared formulations are all close to saturation except d-PG which is freely miscible with water. All the solutions were visibly clear from precipitates at 32 °C, although d-PA was highly viscous at the given temperature.

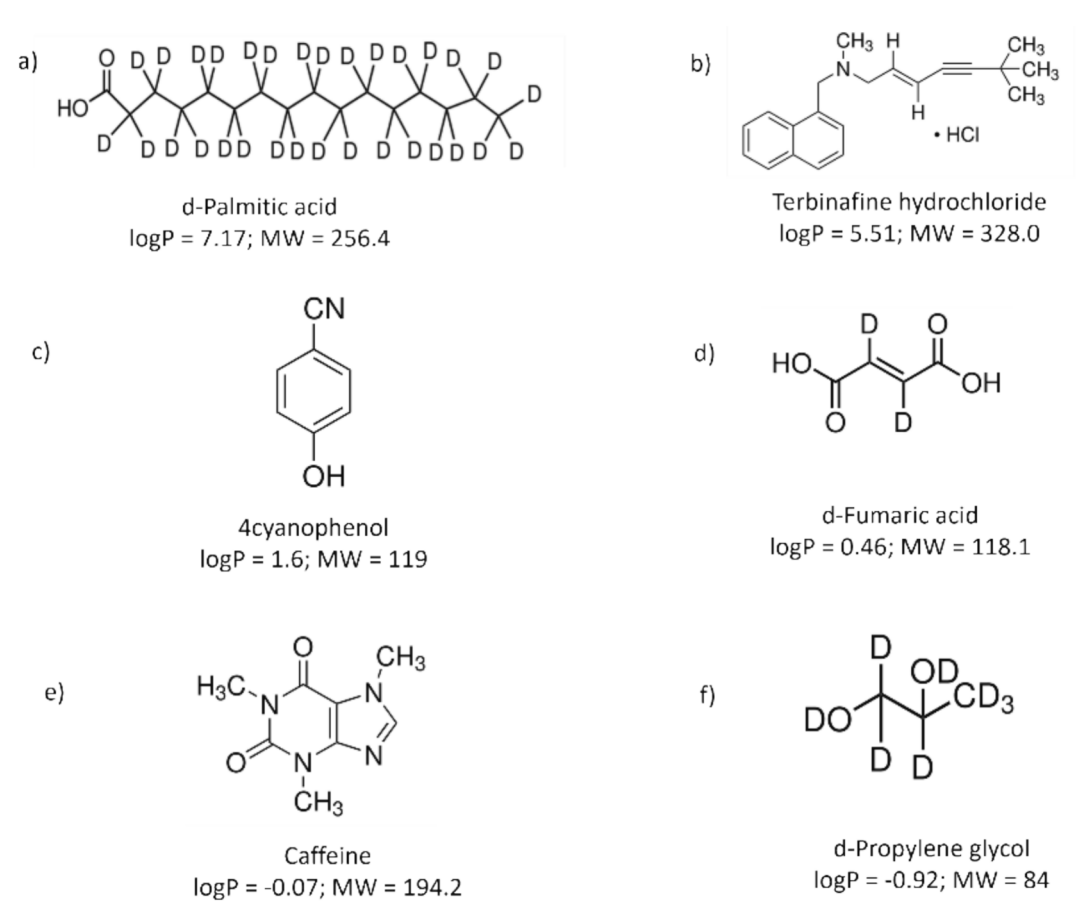


Fig. 1. Chemical structures of the six molecules studied.

2.2. Preparation of skin samples

Excised human skin specimens were procured from ALPHENYX (France). Full thickness skin was obtained from abdominal plastic surgery and was stored at -20 °C until use. Skin was sourced from phototype I and II donors to minimise absorption artefacts from melanin. For skin preparation, the skin samples were thawed, mounted on a vertical Franz diffusion cell and the formulations were topically applied at a temperature of 32 °C in an infinite dose scheme. Conducting experiments at 32 °C allows for consistency with in-vivo conditions, where the skin's temperature is typically maintained in that range [26]. The receptor chamber was filled with 0.01 M phosphate-buffered saline (PBS) solution (Sigma Aldrich, UK), and the donor chamber was sealed with parafilm after adding the test formulation. A diffusion period of 24 h was used for all the formulations except d-PG, where the skin was diffused for 8 h. At the end of penetration study, the formulation was removed using a pipette and the skin surface was gently wiped two to three times with a cotton swab soaked in PBS solution. Following that, the epidermis was isolated from the full-thickness skin by epidermal heat separation of the samples. This was necessary to obtain samples sufficiently thin to perform SRS microscopy in transmission, and therefore, to obtain the best quality images. Epidermal separation was performed by placing the skin in a plastic petri dish which was floated on a 60 °C water bath for 2 min [27]. Subsequently the epidermis was removed manually using tweezers, mounted between glass coverslips (#1.5, Menzel Glasser) and imaged with SRS microscopy, as described

2.3. Imaging skin samples with SRS microscopy

SRS microscopy images were acquired using a Leica SP8 laser scanning microscope (Leica Microsystems, Wetzlar, Germany) coupled to a PicoEmerald-S laser system. The PicoEmerald-S generates two pulsed 2 ps laser beams: a 1031.2 nm Stokes beam which was spatially and temporally overlapped with a tuneable pump beam. The Stokes beam was modulated at 20 MHz and stimulated Raman loss signals were detected using a silicon-based detector and lock-in amplifier (UHFLI, Zurich instruments, Zurich, Switzerland). Images were acquired with a water immersion 25X magnification lens (0.95NA, Leica) used in conjunction with a short working distance air condenser lens (0.9NA, Leica). The laser power was set to 30 % which corresponds to approximately 10 mW for the pump beam and 30 mW for the Stokes beam at the sample.

The tissue microstructure was imaged first by tuning the microscope to the CH₂ symmetrical vibrational stretching mode at 2850 cm⁻¹. This mapping facilitated the characterization of the lipid architecture, crucial for visualising the intercellular matrix within the SC. Subsequently, the laser system was tuned to the Raman active signature of the chemicals of interest, allowing for the mapping of their distribution within the skin. This was achieved by tuning the microscope to either the CD, $C \equiv N$, $C \equiv C$ or CH stretching bands to visualise the distribution of either d-PA, d-PG and d-FA, 4CP, TBF or CAF respectively. The position of the Raman bands of the chemicals were previously determined using confocal Raman spectroscopy, with details of the spectroscopy setup and the Raman profiles of the chemicals provided in the supplementary information. To validate the peaks determined by confocal Raman spectroscopy and ensure accurate interpretation of weak signals, hyperspectral SRS scans were also conducted, to confirm the spectral features of the targeted compounds. Additionally, an off-resonance control image was recorded, and any identified spurious signals were subtracted from their on-resonance counterpart. The pump beam wavelengths, corresponding Raman shifts, vibrational mode assignments, and off-resonance frequencies for skin lipids and the six molecules studied are summarized in Table 1. Typical SRS images acquired during this study were comprised of 512×512 pixels, covering an area of 435.9 \times 435.9 μ m², with a pixel dwell time of 15 μ s and a total

Table 1
Pump beam wavelengths and corresponding Raman shifts, vibrational mode, molecule visualized, and off-resonance (control) frequency used for targeting skin and molecules studied.

Pump beam wavelength (nm)	Raman shift (cm ⁻¹)	Vibrational mode	Molecule visualized	Off resonance frequency (cm ⁻¹)
797.0	2850	CH_2	Skin lipids	2700
847.2	2106	CD	d-PA	2030
838.3	2231	C≡C	TBF	2257
838.0	2235	$C \equiv N$	4CP	2257
833.4	2301	CD	d-FA	2356
779.9	3124	CH	CAF	3083
845.9	2124	CD	d-PG	2027

acquisition time of 3.9 s per image. Subsequently, the acquired images underwent processing as described in the following section.

2.4. Image analysis

Image processing steps were performed using ImageJ [28] software (U. S. National Institutes of Health, Bethesda, Maryland, USA, version 1.52a). In instances specified within the text, off-resonance (control) SRS signal contributions were subtracted from their on-resonance counterparts on a pixel-by-pixel basis utilizing the 'Image calculator' plugin. This was performed to remove any spurious signals that were non-Raman in nature. The imaging datasets for each chemical were manually registered based on the presence of the lipids in the skin using 'Linear Stack alignment with the 'SIFT' ImageJ plugin to minimize the impact of stage drift and any swelling of the tissue. For image presentation, linear look-up tables were employed with 'green' and 'red' false colour schemes to represent skin lipids and model permeants respectively. The resultant overlaid images were generated using the 'colour merge' plugin. As the objective of this work was to elucidate the interplay between molecular properties and their partitioning, the differential uptake of topical compounds was quantified by comparing the SRS signal intensity in lipid-rich and lipid poor regions. The signal intensity in both compartments was computed by averaging pixel intensities across five similar regions of interest in both the lipid matrix and corneocyte cells for each compound of interest. The ratio of the averaged signal intensity in lipid-rich and lipid-poor regions was subsequently quantified and reported as the partition factor.

3. Results

The partitioning of six model permeants in the skin were independently assessed $ex\ vivo$ utilizing SRS microscopy. Fig. 2 illustrates the spatial distribution of permeants close to the surface of the SC alongside the corresponding lipid architecture of the tissue, arranged according to the increasing hydrophilicity of the permeants. Leveraging the morphological insights provided by CH₂ signals, the study examined the differential uptake of permeants in lipid-rich versus lipid-poor compartments. The investigation revealed marked diversity among the six compounds studied.

It is evident that for compounds such as d-PA, TBF, 4CP, and d-FA, partitioning into the intercellular lipid matrix of the SC is more favourable, as inferred from Fig. 2a, 2b, 2c, and 2d respectively. The images with a green false-colour scheme depict the lipid architecture of the skin, whereas the red false-colour scheme represents the distribution of molecules studied within the skin. It is evident from the overlaid images of skin lipids and topical compounds in Fig. 2a to 2d that hydrophobic molecules are predominantly situated within the intercellular lipid matrix between corneocyte cells, in alignment with the tissue's lipid architecture. This observation aligns with the hydrophobic nature of such molecules, rendering the intercellular matrix as the preferred compartment for partitioning of lipophilic molecules [29].

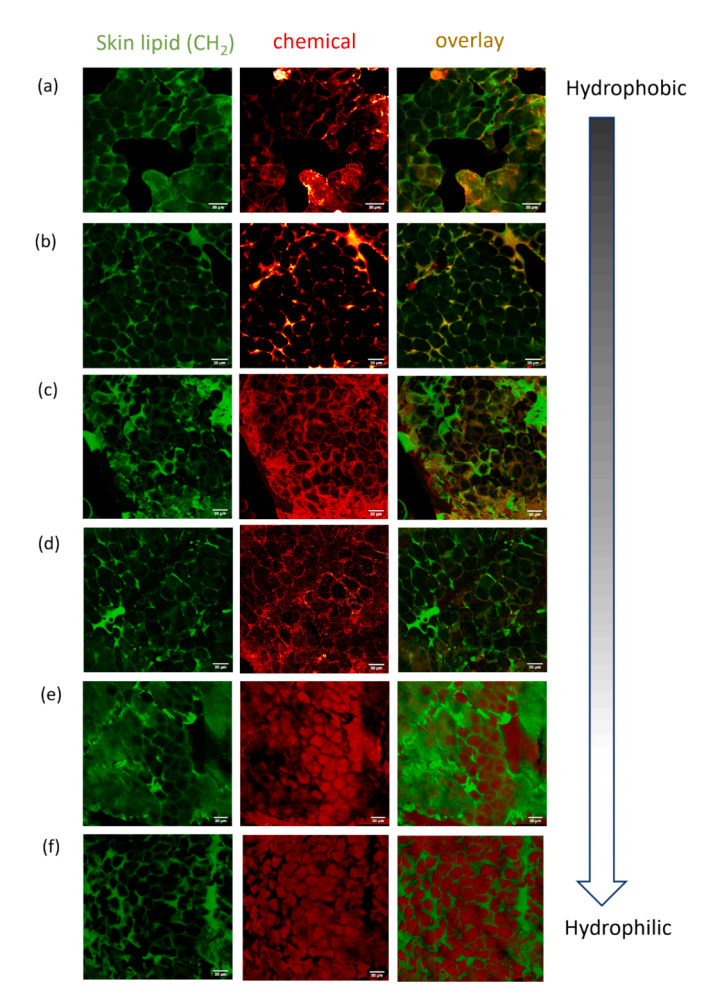


Fig. 2. Representative SRS microscopy images showing the spatial distribution of model permeants in the SC of excised human skin (for optimum comparison, from the same donor, a 32-year-old Caucasian female). Panel (a) d-palmitic acid, (b) terbinafine hydrochloride, (c) 4-cyanophenol, (d) d-fumaric acid, (e) caffeine and (f) d-propylene glycol at the surface of SC. 'Green' false colour scheme represents morphology defined by skin lipid signals, 'red' false colour scheme represents chemical distribution and last column represents overlay of skin lipids and molecules studied. The scale bar represents 30 μm . (For interpretation of the references to colour in this figure legend, the reader is referred to the web version of this article.)

Conversely, molecules such as CAF and d-PG predominantly concentrate within the corneocyte cells, as depicted in Fig. 2e and 2f. In the overlaid images of these two molecules, their distribution appears anticorrelated with the lipid architecture of the skin. This observation can be attributed to the hydrophilic character of d-propylene glycol and caffeine, favouring the water-rich corneocyte cells over intercellular lipids [30]. The absence of a signal in the images of the undosed skin tissue (provided in the Supplementary Information), which was not treated with any molecules of interest, confirms that the distribution mapping of the chemicals originates solely from the topically applied formulation.

To quantify the differential chemical uptake in the two regions, the partition factor for each permeant was determined by its ratio of SRS signal/concentration in lipid-rich and lipid-poor regions (i.e., concentration per volume measured within each phase). The partition factors for the six compounds are depicted in a bubble plot in Fig. 3, where the size of each bubble corresponds to the magnitude of its partition factor. The highest partitioning value is observed for TBF, at 42.40, attributable to its pronounced lipophilic nature. However, a significantly lower partition factor of 2.55 is noted for d-PA, despite its similarly strong

lipophilic characteristics. This discrepancy may stem from the low permeation of d-PA into the skin, giving rise to weak intensity SRS signals compared to the SRS limit of detection, impacting the accuracy of partition factor quantification. The other two hydrophobic molecules, 4CP and d-FA, exhibited average partition factors of 2.57 and 1.95, respectively. Conversely, caffeine and d-PG displayed partitioning values of 0.78 and 0.61, respectively, both below 1.0. This suggests that uptake into the corneocyte cells is preferred over the intercellular lipid matrix.

The experimentally derived partition factors of chemicals within the skin were compared with the model-predicted values developed by Wang *et al*, [31], as detailed in Table 2. These data-based models, which forecast the partition coefficients of solutes into the SC lipid and protein, were employed to predict the partition coefficients for the six compounds under investigation.

The experimentally determined partition coefficients for TBF (42.40) and 4CP (2.57) align closely with the corresponding predicted values from the model (69.50 and 2.11, respectively). However, notable deviations were observed, with d-PA, where the predicted value stands at 310.07, significantly higher than the experimentally assessed value of 2.55. This discrepancy suggests a potential underestimation of the partitioning of d-PA experimentally, possibly due to its poor penetration into the skin resulting in low SRS signals relative to the limit of detection, undermining the partition factor. Interestingly, the partitioning behaviour of d-FA observed experimentally contrasts with the prediction made by the model. The experimental determination yields a partition factor of 1.95 for d-FA, implying a preference to partition into the intercellular matrix. In contrast, the predicted partition value of 0.61 suggests a preference for corneocyte cells. This discrepancy may stem from the underprediction of partition from the model, as observed for certain molecules during model development, thereby altering their partitioning behaviour. Moreover, given the hydrophobic nature of d-FA, it is inclined to show a stronger affinity towards the lipid-rich intercellular matrix, thus reinforcing the significance of the experimental observation. For caffeine, the observed partitioning behaviour aligns closely between experimental and model-predicted values, with partition coefficients of 0.78 and 0.31, respectively. Furthermore, the experimentally determined partition of caffeine was compared with the literature-reported value [32] obtained through a far more invasive and labour-intensive technique. Ellison et al. calculated the partition coefficients in human delipidised SC and SC lipids by direct measurements of the radioactivity in the delipidised tissue layers/lipid component vs. buffer samples. The reported values were used to compute their ratio between lipid-rich and lipid poor SC resulting in a value of 0.79 which is consistent with the findings of this study.

Finally, the partitioning behaviour of d-PG observed in both the experiment and model indicates an affinity towards corneocyte cells, with partition factors of 0.61 and 0.13, respectively. The partitioning behaviour for all molecules (excluding d-FA) appears consistent between the experimental and model-derived results. The disparity in magnitude can be elucidated by the fact that the model was developed from a dataset obtained largely using phosphate-buffered saline (PBS) as the vehicle, based on data deriving from porcine skin as well as human skin. In contrast, this study utilizes human skin to calculate the partition factor in the SC and employs a propylene glycol–water vehicle for most of the molecules resulting in different values of partition [33].

4. Discussion

The study delved into the partitioning of six model permeants within the skin through the application of SRS imaging *in-vitro*. Two-dimensional images were acquired to retrieve information from SC, the outermost layer of skin which is the major barrier to penetration of chemicals. The findings unveiled the spatial distribution of these permeants in the skin alongside the corresponding lipid architecture, revealing the mechanistic preferential partitioning among the

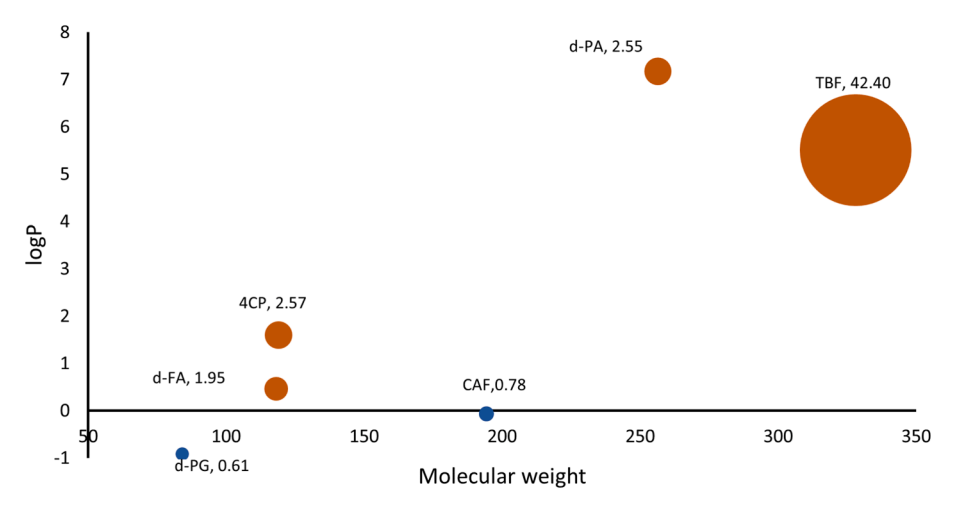


Fig. 3. Bubble plot representing the partition factor for six compounds characterized by their logP and molecular weight. The bubble size corresponds to the magnitude of the partition factor. The orange bubbles are hydrophobic molecules while blue bubbles are hydrophilic molecules. (For interpretation of the references to colour in this figure legend, the reader is referred to the web version of this article.)

Table 2
Comparison of partition factors determined experimentally using SRS imaging with predicted value from data-based model [31] and literature reported data [32].

	Mol. Weight	logP	Experimental partition factor	Model predicted partition factor*	Literature reported partition factor
d-PA	256.4	7.17	2.55 ± 0.44	310	NA
TBF	328.0	5.51	42.40 ± 0.68	69.5	NA
4CP	119.0	1.60	2.57 ± 0.31	2.11	NA
d-FA	118.1	0.46	1.95 ± 0.41	0.61	NA
CAF	194.2	-0.07	0.78 ± 0.25	0.31	0.79**
d-PG	84.0	-0.92	0.61 ± 0.10	0.13	NA

NA - Not available.

compounds studied. Evidently, two distinct permeation pathways through the stratum corneum were visualised: the intercellular lipid matrix and the corneocyte cells. This observation aligns with the widely acknowledged 'brick and mortar model [34], which characterizes waterrich corneocytes (the bricks) embedded within a continuous lipid matrix, akin to mortar illustrating two mechanistic pathways: intercellular and transcellular. The quantification of differential chemical uptake in lipid-rich and lipid-poor pathways elucidated the partitioning behaviour, providing insights into the underlying mechanisms of topical delivery. Overall, the partitioning behaviour is contingent upon the lipophilicity of the molecule. Specifically, hydrophobic compounds exhibited a partition factor greater than 1.0, preferring the intercellular lipid matrix of the SC. Moreover, this preference for intercellular partitioning increased with increase in lipophilicity. Contrarily, the hydrophilic molecules were primarily distributed within the cornecyte cells as revealed by their partition factor less than 1.0 with their inclination toward this compartment increasing with greater hydrophilicity. Experimental findings correlate well with model-predicted partition with some discrepancy, particularly notable with d-FA, underscoring the importance of experimental validation in understanding permeation behaviour. Importantly, it should be noted that while this study reports the relative concentrations of the target molecules measured across the two pathways, it does not report on the relative speed at which they may progress via either route. Moreover, to obtain the best quality SRS images (collected in transmission), epidermal heat separation was necessary to obtain sufficiently thin skin samples. This brief exposure of the skin to 60 °C could affect the SC lipid composition and organization. At elevated temperatures (around 60 °C), these lipids can undergo phase transitions, shifting from an ordered (solid or gel-like) phase to a disordered (liquid crystalline) phase. This disrupts the tightly packed lipid layers, weaking their structural integrity increasing and impairing

the skin's protective barrier [35]. Furthermore, this research uses PG as co-solvent for most of the studied compounds, which is a well-known permeation enhancer. PG disrupts the lipid bilayers of the stratum corneum by altering the ordered structure of skin lipids. By increasing the fluidity of the lipid matrix, propylene glycol can promote the uptake of both hydrophilic and lipophilic molecules. Changes to drug permeation depending on the presence of permeation enhancers has been observed using similar methodology, by Feizpour and coworkers [18]. Nonetheless, this methodology can be adopted to calculate the partition factor in aqueous vehicle and can be used to determine the effect of co-solvents.

To the best of our knowledge this study is the first to systematically investigate different penetration pathways of the topical delivery process for a range of both lipophilic as well as hydrophilic molecules with SRS microscopy. Furthermore, the utilization of human skin samples enhances the clinical relevance of our findings. While SRS microscopy has garnered widespread utilization for *in-vitro* skin permeation studies, ongoing technological advancements hold promise for real-time analysis, positioning SRS as a compelling tool for future *in-vivo* applications [36].

In summary, SRS microscopy emerges as a powerful label-free optical imaging modality, offering unprecedented mechanistic insight into permeation pathways that surpass the capabilities of alternative techniques, which often lack adequate spatial resolution or necessitate the use of bulky labelling agents. Such data is key to furthering our understanding of topical delivery and facilitating the development of innovative and efficacious formulations for dermatological, cosmetic, and pharmaceutical applications. The methods described could provide valuable insight to changes in skin permeation mechanisms in diseased skin models in addition to studying appendageal targeting, paving the way for more efficacious topical therapeutics.

^{*} The model is based on data for skin permeation analysis comprising of piglet skin and human skin using PBS as vehicle.

Partition coefficients of caffeine in SC lipids and delipidised SC were used for deriving partition factor.

Ethics statement

Research ethics approval was obtained from University of Surrey's Ethics Committee (FEPS 20–21 001 EGA).

Funding Sources

This work was funded by the National Centre for the Replacement, Refinement and Reduction of Animals in Research, UK (NC3Rs, grant number NC/T001720/1) and Unilever, UK. It was also part-funded by the UK Department of Science Innovation & Technology through the National Measurement System programme. This work was also supported by the Community for Analytical Measurement Science through a 2020 CAMS Fellowship Award to Natalie Belsey funded by the Analytical Chemistry Trust Fund.

CRediT authorship contribution statement

Anukrati Goel: Writing – original draft, Visualization, Methodology, Investigation. Ruth Pendlington: Writing – review & editing, Supervision. Stephen Glavin: Writing – review & editing, Supervision. Tao Chen: Writing – review & editing, Supervision, Funding acquisition, Conceptualization. Natalie A. Belsey: Writing – review & editing, Supervision, Methodology, Funding acquisition, Conceptualization.

Declaration of Competing Interest

The authors declare that they have no known competing financial interests or personal relationships that could have appeared to influence the work reported in this paper.

Data availability

Data will be made available on request.

Appendix A. Supplementary material

Supplementary data to this article can be found online at https://doi. org/10.1016/j.ejpb.2024.114518.

References

- T. Chen, G. Lian, P. Kattou, In silico modelling of transdermal and systemic kinetics of topically applied solutes: model development and initial validation for transdermal nicotine. Pharm. Res. 33 (2016) 1602–1614.
- [2] P.M. Elias, Structure and function of the stratum corneum permeability barrier, Drug Dev. Res. 13 (2–3) (1988) 97–105.
- [3] A. Zaid Alkilani, M.T. McCrudden, R.F. Donnelly, Transdermal drug delivery: Innovative pharmaceutical developments based on disruption of the barrier properties of the stratum corneum, Pharmaceutics 7 (4) (2015) 438–470.
- [4] Y.-C. Kim, J.-H. Park, M.R. Prausnitz, Microneedles for drug and vaccine delivery, Adv. Drug Deliv. Rev. 64 (14) (2012) 1547–1568.
- [5] N.J. Everall, Confocal Raman microscopy: common errors and artefacts, Analyst 135 (10) (2010) 2512–2522.
- [6] P.J. Caspers, H.A. Bruining, G.J. Puppels, G.W. Lucassen, E.A. Carter, In vivo confocal Raman microspectroscopy of the skin: noninvasive determination of molecular concentration profiles, J, Invest. Dermatol. 116 (3) (2001) 434–442.
- [7] G. Mao, C. Flach, R. Mendelsohn, R. Walters, Imaging the distribution of sodium dodecyl sulfate in skin by confocal Raman and infrared microspectroscopy, Pharm. Res. 29 (2012) 2189–2201.
- [8] P. Berto, E.R. Andresen, H. Rigneault, Background-free stimulated Raman spectroscopy and microscopy, Phys. Rev. Lett. 112 (5) (2014) 053905.
- [9] A.-M. Pena, X. Chen, I.J. Pence, T. Bornschlögl, S. Jeong, S. Grégoire, G.S. Luengo, P. Hallegot, P. Obeidy, A. Feizpour, Imaging and quantifying drug delivery in

- skin–Part 2: fluorescence and ibrational spectroscopic imaging methods, Adv. Drug Deliv. Rev. 153 (2020) 147–168.
- [10] C. Krafft, I.W. Schie, T. Meyer, M. Schmitt, A.J. Popp, Developments in spontaneous and coherent Raman scattering microscopic imaging for biomedical applications, Chem. Soc. Rev. 45 (7) (2016) 1819–1849.
- [11] D. Zhang, Q. Bian, Y. Zhou, Q. Huang, J. Gao, The application of label-free imaging technologies in transdermal research for deeper mechanism revealing, Asian J. Pharm. Sci. 16 (3) (2021) 265–279.
- [12] B.G. Saar, L.R. Contreras-Rojas, X.S. Xie, R.H. Guy, Imaging drug delivery to skin with stimulated Raman scattering microscopy, Mol. Pharm. 8 (3) (2011) 969–975.
- [13] L. Wei, F. Hu, Z. Chen, Y. Shen, L. Zhang, W. Min, Live-cell bioorthogonal chemical imaging: stimulated Raman scattering microscopy of vibrational probes, Acc. Chem. Res. 49 (8) (2016) 1494–1502.
- [14] X. Chen, S. Grégoire, F. Formanek, J.-B. Galey, H. Rigneault, Quantitative 3D molecular cutaneous absorption in human skin using label free nonlinear microscopy, J. Control. Release 200 (2015) 78–86.
- [15] M. Cicerone, Molecular imaging with CARS micro-spectroscopy, Curr. Opin. Chem. Biol. 33 (2016) 179–185.
- [16] B. Sarri, X. Chen, R. Canonge, S. Grégoire, F. Formanek, J.-B. Galey, A. Potter, T. Bornschlögl, H. Rigneault, In vivo quantitative molecular absorption of glycerol in human skin using coherent anti-Stokes Raman scattering (CARS) and twophoton auto-fluorescence, J. Control. Release 308 (2019) 190–196.
- [17] N.A. Belsey, N.L. Garrett, L.R. Contreras-Rojas, A.J. Pickup-Gerlaugh, G.J. Price, J. Moger, R.H. Guy, Evaluation of drug delivery to intact and porated skin by coherent Raman scattering and fluorescence microscopies, J. Control. Release 174 (2014) 37–42.
- [18] A. Feizpour, T. Marstrand, L. Bastholm, S. Eirefelt, C.L. Evans, Label-free quantification of pharmacokinetics in skin with stimulated Raman scattering microscopy and deep learning, J, Invest. Dermatol. 141 (2) (2021) 395–403.
- [19] E.C. Jung, H.I. Maibach, Animal models for percutaneous absorption, Topical drug bioavailability, bioequivalence, and Penetration (2014) 21–40.
- [20] C. Choe, J. Schleusener, J. Lademann, M.E. Darvin, Human skin in vivo has a higher skin barrier function than porcine skin ex vivo—comprehensive Raman microscopic study of the stratum corneum, J. Biophotonics 11 (6) (2018) e201700355.
- [21] M.J. Visconti, W. Haidari, S.R. Feldman, Therapeutic use of caffeine in dermatology: a literature review, J. Dermatol. Dermatol. Surg. 24 (1) (2020) 18–24.
- [22] M. Panday, D. Pandey, P. Upadhyay, S. Upadhyay, Terbinafine preferred antifungal with a focus on dermatophytes (a review), Acta. Sci. Microbiol. 3 (2020) 65–72.
- [23] A.M. Rabasco Álvarez, M.L. González Rodríguez, Lipids in pharmaceutical and cosmetic preparations, Grasas Aceites 51 (1–2) (2000) 74–96.
- [24] M.A. McGowan, A. Scheman, S.E. Jacob, Propylene glycol in contact dermatitis a systematic review, Dermatitis 29 (1) (2018) 6–12.
- [25] A. Goel, D. Tsikritsis, N.A. Belsey, R. Pendlington, S. Glavin, T. Chen, Measurement of chemical penetration in skin using Stimulated Raman scattering microscopy and multivariate curve resolution-alternating least squares, Spectrochim. Acta A Mol. Biomol. Spectrosc. 296 (2023) 122639
- [26] OECD. OECD Guidelines for the Testing of Chemicals; Oecd, 1994.
- [27] Y. Zou, H.I. Maibach, Dermal-epidermal separation methods: research implications, Percutaneous Absorption (2021) 885–896.
- [28] C.T. Rueden, J. Schindelin, M.C. Hiner, B.E. DeZonia, A.E. Walter, E.T. Arena, K. W. Eliceiri, Image J2: IMAGEJ for the next generation of scientific image data, BMC Bioinf. 18 (2017) 1–26.
- [29] M.-A. Bolzinger, S. Briançon, J. Pelletier, Y. Chevalier, Penetration of drugs through skin, a complex rate-controlling membrane, Curr. Opin. Colloid Interface Sci. 17 (3) (2012) 156–165.
- [30] J.W. Wiechers, The barrier function of the skin in relation to percutaneous absorption of drugs, Pharm. Weekbl. 11 (1989) 185–198.
- [31] L. Wang, L. Chen, G. Lian, L. Han, Determination of partition and binding properties of solutes to stratum corneum, Int. J. Pharm. 398 (1–2) (2010) 114–122.
- [32] C.A. Ellison, K.O. Tankersley, C.M. Obringer, G.J. Carr, J. Manwaring, H. Rothe, H. Duplan, C. Géniès, S. Grégoire, N.J. Hewitt, Partition coefficient and diffusion coefficient determinations of 50 compounds in human intact skin, isolated skin layers and isolated stratum corneum lipids, Toxicol. In Vitro 69 (2020) 104990.
- [33] S. Songkro, An overview of skin penetration enhancers: penetration enhancing activity, skin irritation potential and mechanism of action, Songklanakarin J. Sci. Technol. 31 (3) (2009).
- [34] P.M. Elias, Epidermal lipids, barrier function, and desquamation, J, Invest. Dermatol. 80 (1) (1983) S44–S49.
- [35] J.A. Bouwstra, M. Ponec, The skin barrier in healthy and diseased state, Biochimica et Biophysica Acta (BBA)-Biomembranes 1758 (12) (2006) 2080–2095.
- [36] D. Tsikritsis, E.J. Legge, N.A. Belsey, Practical considerations for quantitative and reproducible measurements with stimulated Raman scattering microscopy, Analyst 147 (21) (2022) 4642–4656.